tvst

Article

A Two-Stage Laser-Induced Mouse Model of Subretinal Fibrosis Secondary to Choroidal Neovascularization

Karis Little[1], María Llorián-Salvador[1], Miao Tang[1], Xuan Du[1], Órlaith O'Shaughnessy[1], Gemma McIlwaine[1], Mei Chen[1], and Heping Xu[1]

[1] The Welcome-Wolfson Institute for Experimental Medicine, School of Medicine, Dentistry and Biomedical Sciences, Queen's University Belfast, Belfast, UK

Correspondence: Heping Xu, The Welcome-Wolfson Institute for Experimental Medicine, Queen's University Belfast, 97 Lisburn Road, Belfast, UK BT9 7BL. e-mail: heping.xu@qub.ac.uk

Received: August 12, 2019
Accepted: November 20, 2019
Published: March 9, 2020

Keywords: subretinal fibrosis; neovascularization; inflammation

Citation: Little K, Llorián-Salvador M, Tang M, Du X, O'Shaughnessy Ó, McIlwaine G, Chen M, Xu H. A two-stage laser-induced mouse model of subretinal fibrosis secondary to choroidal neovascularization. Trans Vis Sci Tech. 2020;9(4):3, https://doi.org/10.1167/tvst.9.4.3

Purpose: To develop a model that can recapitulate key features of macular fibrosis in neovascular age-related macular degeneration (nAMD).

Methods: Adult C57BL/6J mice received three laser burns/eye to induce choroidal neovascularization (CNV). Seven days later, a second laser burn was directed to each of the neovascular lesions. Traditional laser-induced CNV was used as a control. Lesions were monitored at 10, 20, 30, and 40 days post-laser (p.l) treatment by fundus imaging, fundus fluorescein angiography, optical coherence tomography (OCT), and immunohistochemistry. The expression of collagen-1 (COL-1), fibronectin, α-smooth muscle actin, F4/80, complement factor B (CFB), Complement component 3 (C3), transforming growth factor-β (TGF-β), and fibroblast growth factor 2 (FGF2) in retina and retinal pigment epithelium/choroid was examined by immunofluorescence and reverse transcription polymerase chain reaction.

Results: The two-stage laser protocol induced significantly larger lesions than the traditional laser-CNV by OCT and immunohistochemistry at all time points. Confocal microscopy detected COL-1$^+$ fibers and IBA1$^+$/CD31$^+$ blood vessels in lesions from the two-stage laser protocol 30 to 40 days p.l. Lesions from traditional laser-CNV contain only COL-1$^+$ fibers but not blood vessels at this time point. Higher levels of proinflammatory (inducible nitric oxide synthase (iNOS), C3, CFB) and profibrotic (TGF-β, FGF2, and vascular endothelial growth factor) genes were detected in the retinas from the two-stage laser-induced lesions compared with the traditional laser-CNV lesion. Higher number of infiltrating F4/80 macrophages was also observed in and around the two-stage laser-induced fibrotic lesion.

Conclusions: The two-stage laser treatment induced subretinal fibrovascular membranes that persist over 40 days.

Translational Relevance: The model is a useful tool to study the mechanism of macular fibrosis in nAMD and test antifibrotic drugs.

Introduction

Age-related macular degeneration (AMD) is the leading cause of blindness in those over the age of 50 years in the developed world, and is estimated to affect 196 million people by 2020.[1] "Wet" AMD, also termed neovascular AMD (nAMD), is characterized by the growth of abnormal blood vessels arising from the choroid (e.g., choroidal neovascularization [CNV], or polypoidal choroidal vasculopathy) or the retina—retinal angiomatous proliferation. This can cause rapid vision loss. The end stage of nAMD is macular fibrosis, which leads to irreparable vision loss.

Clinically, macular fibrosis is presented as a well-demarcated, elevated mound of white/yellowish material within or underneath the retina,[2] which often contain blood vessels.[3,4] The standard treatment for nAMD is the intravitreal injection of anti-vascular endothelial growth factor (VEGF) agents, however, it was shown that after 2 years of treatment, 45% of eyes developed scarring.[5] The molecular mechanisms

involved in the development of subretinal fibrosis in nAMD are unknown.

To dissect the mechanism of subretinal fibrosis secondary to nAMD, and to investigate therapeutic strategies, a suitable animal model is necessary. The laser-induced CNV model, first described in mice by Tobe et al. in 1998,[6,7] is useful to replicate CNV in nAMD, however, the CNV membrane formed has been reported to spontaneously regress 3 weeks after CNV induction.[7] Ishikawa et al.[8] showed that the CNV at the late stage (>35 days post-CNV induction) becomes an α-smooth muscle actin (α-SMA)$^+$ fibrotic lesion. This model has since been used to research mechanisms of retinal fibrosis[9–11] and to test antifibrotic drugs.[12] However, lesions in this model do not contain blood vessels, therefore do not truly replicate macular fibrosis in nAMD.

Jo et al.[13] combined the laser-induced CNV with a subretinal injection of macrophage-rich peritoneal exudate cells resulting in exacerbated retinal fibrosis. However, the model is technically challenging and difficult to reproduce.

Clinical studies have shown that refractory intraretinal cysts[14] and macular haemorrhage[15] increase the risk of macular fibrosis. We hypothesize that severe vascular leakage or hemorrhage from CNV may result in immune cell infiltration and profibrotic cytokine and chemokine production. These infiltrating cells and profibrotic cytokines are important for the transition of the neovascular lesion to a fibrovascular membrane. Based on this hypothesis, we developed a model whereby the laser-induced CNV was subjected to a second laser burn to induce leakage or bleeding, which then converts the CNV into a fibrovascular membrane.

Methods and Materials

Animals

C57BL/6J mice aged between 2 and 3 months were used in this study. All animals were housed and bred in a standard experimental facility and exposed to a 12 hour light/dark cycle with free access to food and water. All procedures were conducted under the regulation of the United Kingdom Home Office Animals Scientific Research Act 1986 and in accordance with the ARVO Statement for the Use of Animals in Ophthalmic and Vision Research.

Two-Stage Laser Model

Pupils were dilated using atropine (1% w/v) and phenylephrine hydrochloride (2.5% w/v) (Chauvin, Essex, UK). Mice were anesthetized with ketamine hydrochloride (60 mg/kg) (Fort George Animal Centre, Southampton, UK) and xylazine (5 mg/kg) (Pharmacia & Veterinary Products, Kiel, Germany) via intraperitoneal injection. Liquid gel eye drops (Viscotears; Novartis Pharmaceuticals Ltd., Surrey, UK) were used to moisten the ocular surface.

Stage one: Laser-CNV was carried out as previously described[7] using a laser photocoagulator (HGM Medical Laser Systems Inc., Salt Lake City, USA). Three laser burns were carried out in each eye at 3, 6, and 9 o'clock positions of the fundus, approximately 1 disc diameter from the optic nerve. Laser settings were 250 mv power, 0.1s duration, and 100 µm spot size. Lesions that were bleeding after initial laser burn were not included for stage two of the model, or for further study. The day of laser (CNV induction) was considered as day −7 in the two-stage laser group of this study.

Stage two: 7 days later (day 0), a second laser burn was applied. The laser beam was aimed at the CNV lesion created 1 week previously, which is visualized as a whitish/yellowish spot on the fundus. Laser settings were the same as the first laser treatment. After second laser burn, the lesion was either classified as "bleeding" (a small-scale hemorrhage is observed at the lesion site), or "nonbleeding" (no blood is observed after laser injury). In both cases, a fibrotic lesion was formed over the course of 40 days.

The control group received one laser burn, that is, the traditional laser-CNV model.

In Vivo Imaging

Lesions were observed at 10, 20, 30, and 40 days post-laser (p.l) or second laser injury using optical coherence tomography (OCT), and fundus fluorescein angiography (FFA). OCT scans were conducted using the spectral domain-OCT system (Heidelberg Engineering Ltd., Hertfordshire, UK). Scans were performed in the lesion areas. Multiple scans were taken across the entire lesion and used to measure the lesion at its maximal point, using the Heidelberg eye explorer software. Fundus images and FFA were collected using the micron IV system (Pheonix Technology Group, California, USA). FFA images were taken within 5 minutes after intraperitoneal injection of 100 µL of 10% sodium fluorescein.

Leakage from the lesion was measured using Image J software (National Institutes of Health, Bethesda, MD). Area and mean gray value of each lesion were measured. Mean gray value per lesion was compared between laser-CNV and two-stage laser groups. OCT

images were used to measure the area and depth of each lesion.

Histology Staining

Eyes were enucleated at 10, 20, 30, and 40 days p.l (or second laser) and fixed for 2 hours at room temperature (RT) in 2% paraformaldehyde (PFA). Eyes were processed for paraffin-wax embedded sectioning, cryosectioning or flatmount staining. Hematoxylin and eosin (H&E) staining was carried out using the standard protocol. Masson's trichrome staining was performed using a trichrome staining kit (Abcam, Cambridge, UK, Cat no: ab150686).

Retinal Pigment Epithelium (RPE)/Choroid Flatmount Staining

Eyes were enucleated at 10, 20, 30, and 40 days p.l (or second laser) and fixed for 2 hours at RT in 2% PFA. RPE/choroid flatmounts were dissected under a microdissection microscope (Nikon smz800, Nikon, Tokyo, Japan) using a protocol described previously by us.[16] RPE/choroid tissues were washed in phosphate-buffered saline (PBS) followed by treatment with 1% Triton-X 100 for 2 hours at RT. After washing, samples were blocked with 5% bovine serum albumin in 0.1% Triton-X 100 for 1 hour at RT, and then incubated with primary antibody (rabbit anti-mouse collagen-1, Abcam, dilution 1:100; rat anti-mouse F4/80, Bio-Rad, California, USA, 1:100; Isolectin-B4 [IB4] FITC conjugated, Vector Labs, California, USA, 1:50) overnight at 4°C. After thorough washes, samples were incubated with secondary antibody (goat anti-rabbit Alexa Fluor 594 conjugated, Life Technologies (California, USA), 1:200 or donkey anti-rat 488 conjugated, Life Technologies, 1:200) for 2 hours at RT, followed by 3 × 10 minute PBS washes. Flatmounts were mounted with vectashield imaged at 10x magnification on the Dmi8 fluorescence microscope (Leica Camera, Wetzlar, Germany). Collagen-1 $(COL\text{-}1)^{+}/IB4^{+}$ area was measured using Image J by two independent blinded researchers.

Cryosections were stained for COL-1 in a similar fashion, with 1% Triton-X applied for 15 minutes, and primary and secondary antibody incubations taking place at RT for 1 hour. IB4 was incubated for 1 hour at RT. Further characterization was carried out using rat anti-mouse CD31, (Thermofisher, Massachusetts, USA, 1:100) and rabbit anti-mouse fibronectin (Abcam, 1:100). Imaging was carried out using the Dmi8 fluorescence microscope (Leica Camera).

Reverse Transcription Polymerase Chain Reaction (RT-PCR)

RT-PCR was carried out on RNA extracted from the retina and RPE/choroid layer 25 days p.l/post-second laser using the RNEasy mini kit (Qiagen, Hilden, Germany). Lysis buffer was supplemented with 1% β-mercaptoethanol. Each group contained 3 to 4 mice (6–8 eyes). Baseline levels of gene expression were tested in RNA from retina and RPE/choroid from 3-month-old C57Bl6 mice (untreated) n = 6 eyes. cDNA was generated using a reverse transcriptase kit (Thermofisher). Primer sequences are shown in Table 1. Taqman probes are shown in Table 2.

Results

Clinical Feature of Retinal Lesion Following Two-Stage Laser Treatment

Lesions created by the two-stage laser protocol were compared with the lesions from the traditional one laser-induced CNV clinically and histopathologically at 10, 20, 30, and 40 days p.l. FFA showed significant fluorescein leakage from retinal lesions at 10 days p.l in the one-stage laser-induced CNV model, and the leakage declined from days 20 to 40 p.l (Figs. 1A, 1D). In the two-stage laser model, approximately one-third of all lesions had hemorrhage (Fig. 1B) after the second laser, and the remaining two-thirds did not have hemorrhage (Fig. 1C). When all lesions from the two-stage laser model were pooled together (regardless of the hemorrhage), there was a reduction in the size of FFA leakage from day 10 to 30, but the lesion increased again on day 40 p.l (Figs. 1B–D). The lesion size in FFA examination from the two-stage laser model was significantly larger compared with that from the traditional laser-CNV model at each time point (Figs. 1B–D). There was no difference in the level of FFA leakage between lesions with hemorrhage (Fig. 1B) and those without hemorrhage following second laser (Figs. 1C, 1E).

OCT examination showed that the lesions were located at the outer layers of the retina (Figs. 2A, 2B). The depth (Fig. 2A) and area (Fig. 2B) were measured using OCT images scanned through the central lesion area (ascertained by taking multiple OCT images throughout the lesion to identify the maximal depth). The lesion size reduces from days 20 to 40 in the traditional one laser-induced CNV model but not the two-stage laser-induced model (Figs. 2E, 2F). The area of the retinal lesion was significantly larger in the two-stage laser model (Figs. 2D, 2E) compared with those in

Table 1. Primer Sequences for Quantitative PCR

Gene	Forward Sequence	Reverse Sequence
GAPDH	TGGCAAAGTGGAGATTGTTGC	AAGATGGTGATGGGCTTCCCG
α-SMA	TGGCACCACTCTTTCTATAACG	GGTCATTTTCTCCCGGTTGG
Fibronectin	CCACTTCCCCTTCCTGTACA	ATCGTAGTTCTGGGTGGTGC
COL-1	GTGGCGGTTATGACTTCAGC	GGCTGCGGATGTTCTCAATC
CFB	CTCGAACCTGCAGATCCAC	TCAAAGTCCTGCGGTCGT
C3	ACCTTACCTCGGCAAGTTTCT	CTGCTGGTCAGGCTCCTC
iNOS	GGCAAACCCAAGGTCTACGTT	TCGCTCAAGTTCAGCTTGGT

Table 2. TaqMan Probes for Quantitative PCR

TaqMan Probe	Cat. No (Roche)
18s	307906
FGF2	313918
VEGF-a	314944
TGF-β	317139

the traditional one laser-induced CNV model at all time points (Figs. 2C, 2E). The depth of the retinal lesion was significantly larger in the two-stage laser model at 40 days p.l. compared with the laser-induced CNV model (Fig. 2F). We observed no significant differences between bleeding and nonbleeding lesions in terms of lesion area (Fig. 2G) or depth (Fig. 2H).

Histology of Retinal Lesion

H&E staining showed that the lesions were located between photoreceptors and choroid, that is, subretinal space, (Fig. 3A) and contained cells and extracellular matrix (yellow arrow, Fig. 3A). Masson's trichrome staining revealed a significant amount of collagen deposition within the lesion from 10 (blue area, white arrow in Fig. 3B) and 40 (Fig. 3C, white arrow) days p.l, suggesting fibrotic nature of the lesions. Subretinal lesions were also detected in the traditional laser-CNV model 10 days p.l (Fig. 3D, white arrow) and contained collagen fibers (Fig. 3E). Small collagen$^+$ lesions were also detected 40 days p.l, (Fig. 3F, white arrow).

Immunophenotype of Subretinal Lesion

COL-1 deposition in the subretinal lesion was further confirmed by immunostaining of RPE/choroid flatmounts (Fig. 4). COL-1$^+$ lesions were detected at all time points from both the traditional laser-induced CNV (Fig. 4A) and the two-stage laser model (Fig. 4B), although the lesion size was significantly larger in the two-stage laser-induced model compared with the traditional laser-induced CNV model (Fig. 4C). In the traditional laser-induced CNV, the lesion size slightly declined from day 10 to 20 and remained stable from days 20 to 40 (Fig. 4A). In the two-stage laser-induced fibrosis model, the lesion size reduced from day 10 to 20 (Figs. 4B, 4C), but increased again on day 30 (0.18 mm^2) and remained stable until the end of the experiment (i.e., day 40; Fig. 4C).

To further characterize the lesion, RPE/choroidal flatmounts were stained with IB4, which stains both blood vessels and infiltrating macrophage/microglia. The maximum size of the IB4$^+$ lesion in the traditional one laser-induced model (Fig. 5A) was observed at day 10, the lesion size decreased over time and negligible levels of IB4$^+$ were detected at day 40 after laser injury (Figs. 5A, 5C). In the two-stage laser-induced model (Fig. 5B), the IB4$^+$ lesions were detected at all time points and the lesions were significantly larger than those in traditional one laser-induced model (Figs. 5B, 5C). The maximum size of IB4$^+$ lesion was observed at day 10, and the lesion size decreased from days 20 and 30 but increased again on day 40 (Fig. 5C).

In line with RPE/choroidal staining, staining of mouse eye cryosections showed very few IB4$^+$ vessels in the traditional laser-induced subretinal lesion at 30 days p.l (Fig. 5D, white arrows), whereas the two-stage laser model lesion contains numerous blood vessels at this time point (Fig. 5E, yellow arrows). This result was further confirmed by dual staining for CD31 and fibronectin (Fig. 5F). These data suggest that the lesion formed in the two-stage laser model is fibrovascular, with a significant amount of new blood vessels that do not regress by 40 days.

Inflammation in Subretinal Fibrovascular Lesions

Based on our hypothesis, the second laser induces leakage or hemorrhage from preexisting CNV, which would cause more severe inflammation. RT-PCR of

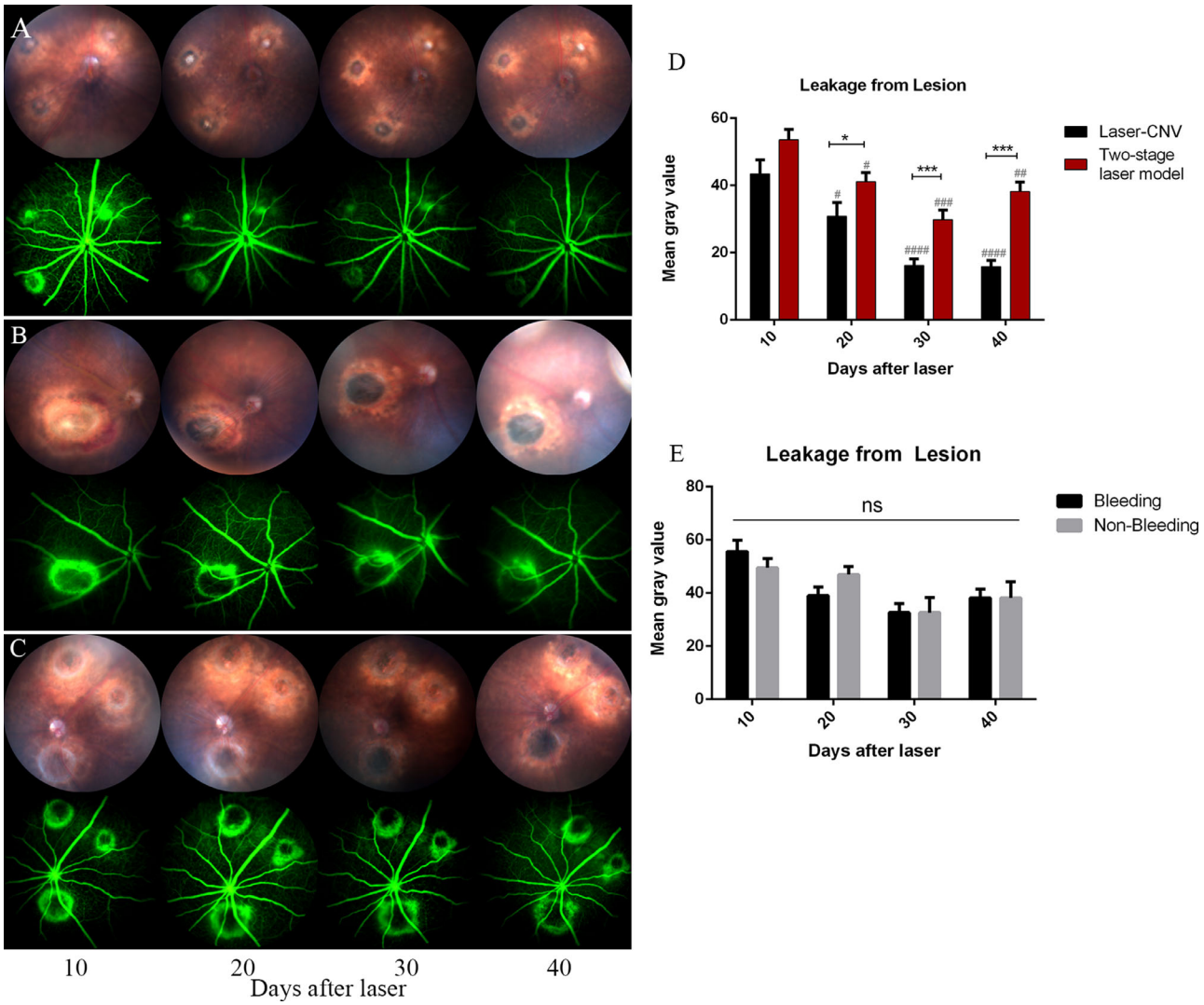

Figure 1. Fundus images and fluorescein angiography of subretinal lesion. Fundus photography and FFA were conducted 10, 20, 30, and 40 days after laser/after second laser. (A) Fundus (upper panel) and FFA (lower panel) images from the traditional laser-CNV at different days. (B) Fundus (upper panel) and FFA (lower panel) images of a lesion at different days from two-stage laser model with hemorrhage induced by the second laser. (C) Fundus (upper panel) and FFA (lower panel) images showing lesions at different days from the two-stage laser model without hemorrhage. (D) Fluorescein leakage in the laser-CNV and two-stage laser model expressed as mean of gray value. Mean ± SEM, N = 6. The Student's *t*-test was used when comparing the two models at the same time point. *Significant difference between laser-CNV and two-stage laser model. *$P < 0.05$; ***$P < 0.005$. One-way ANOVA was used followed by Bonferroni's multiple comparisons when compared day 10 with other time points of the same group. #Significant difference versus 10 days. #$P < 0.05$; ##$P < 0.01$; ###$P < 0.005$; ####$P < 0.001$. (E) The FFA leakage between bleeding and nonbleeding lesions at different time points. Bleeding n = 5, nonbleeding n = 10.

retinas from 25 days p.l (or post-second laser) treatment showed that the expression levels of iNOS and complement C3 were significantly increased in the two-stage laser-induced lesions compared with the traditional one laser-induced lesions (Fig. 6A). A significant upregulation of complement factor B (CFB) was also seen compared with untreated controls. Many F4/80$^+$ macrophages were detected in RPE/choroidal flatmounts from day 30 p.l two-stage laser-induced fibrosis model inside the lesion (Fig. 6B), as well as around the lesion (Fig. 6C). Occasionally, a few F4/80 macrophages were detected in RPE/choroidal flatmounts near the lesion, but not inside the lesion, in the traditional laser-induced CNV at day 30 p.l (Fig. 6C).

The gene expression of transforming growth factor-β (TGF-β), fibroblast growth factor 2 (FGF2), and VEGF-a was increased in the retinas 25 days p.l, although the increment was more significant in eyes from the two-stage laser model (Fig. 7A). Significantly

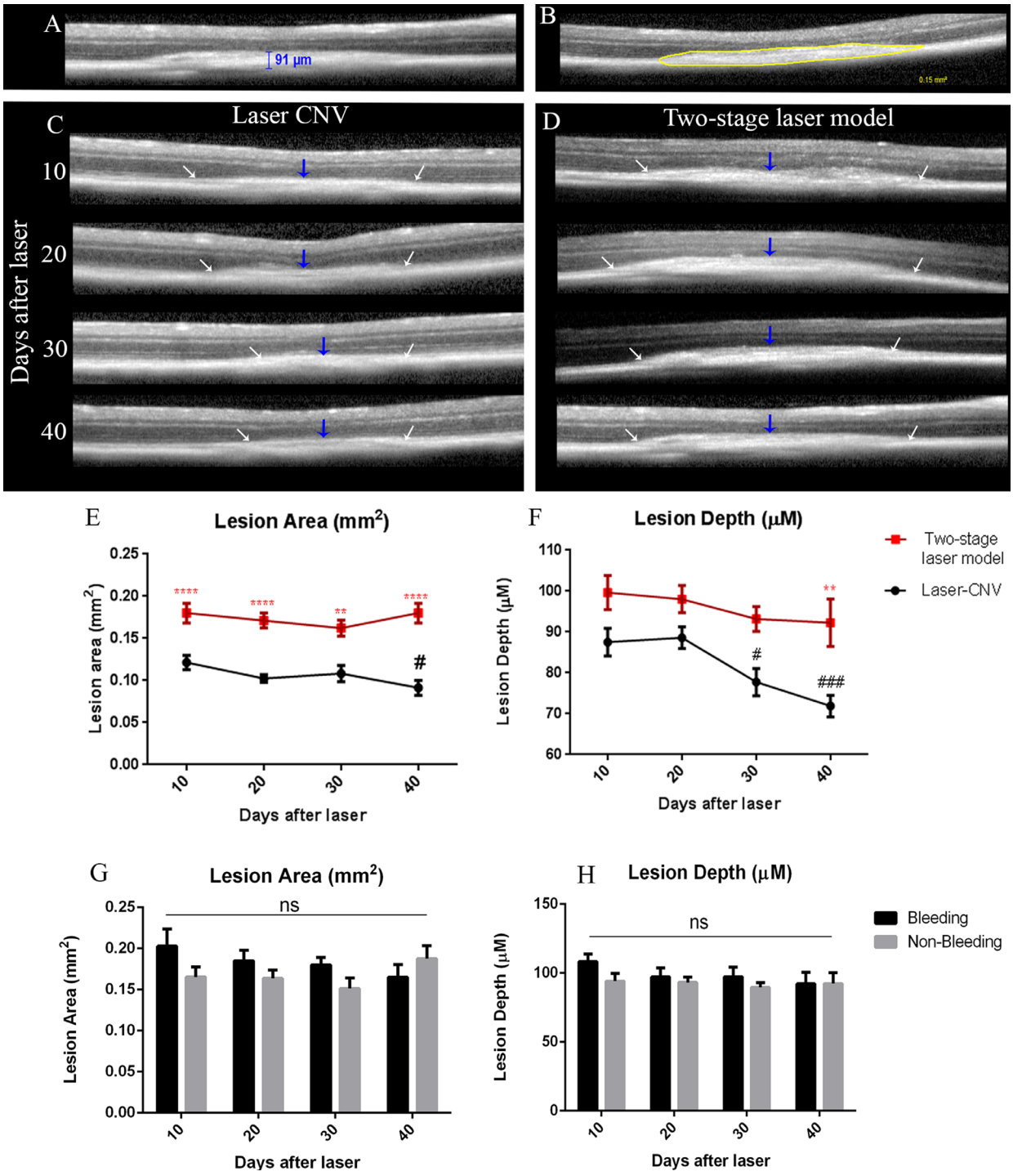

Figure 2. Subretinal lesion from laser-CNV and the two-stage laser model detected by OCT. Retinal lesions were imaged using Heidelberg OCT at different days after the laser/second laser treatment. (A) Depth of lesion was measured at the maximal lesion size from the base of the choroid to the uppermost border of the lesion. (B) The border of the lesion was seen to slope up from the RPE/choroid area, and lesion area was measured based on the border. Yellow border depicts lesion area. (C, D) Representative OCT images from the laser-CNV (C) and the two-stage laser group (D) at different days. White arrows depict lesion borders. Blue arrow depicts center of the lesion. (E) Comparison of lesion area and (F) comparison of lesion depth. Mean ± SEM. $^{**}P < 0.01$; $^{***}P < 0.001$ between laser-CNV and two-stage laser model at the same time point, $\#P < 0.05$; $\#\#\#P<0.001$ versus 10 days of the same group. Two-way ANOVA, Bonferroni corrected, 12 to 30 spots per group from 4 to 6 mice/group. (G) Bar figure showing lesion size (area) at different time points between lesions with hemorrhage and lesions without hemorrhage after the second laser. (H) Bar figure showing lesion depth at different time points between lesions with hemorrhage and lesions without hemorrhage after the second laser. Mean ± SEM. Bleeding n = 5, nonbleeding n = 10. Statistical analysis: one-way ANOVA, Bonferroni corrected.

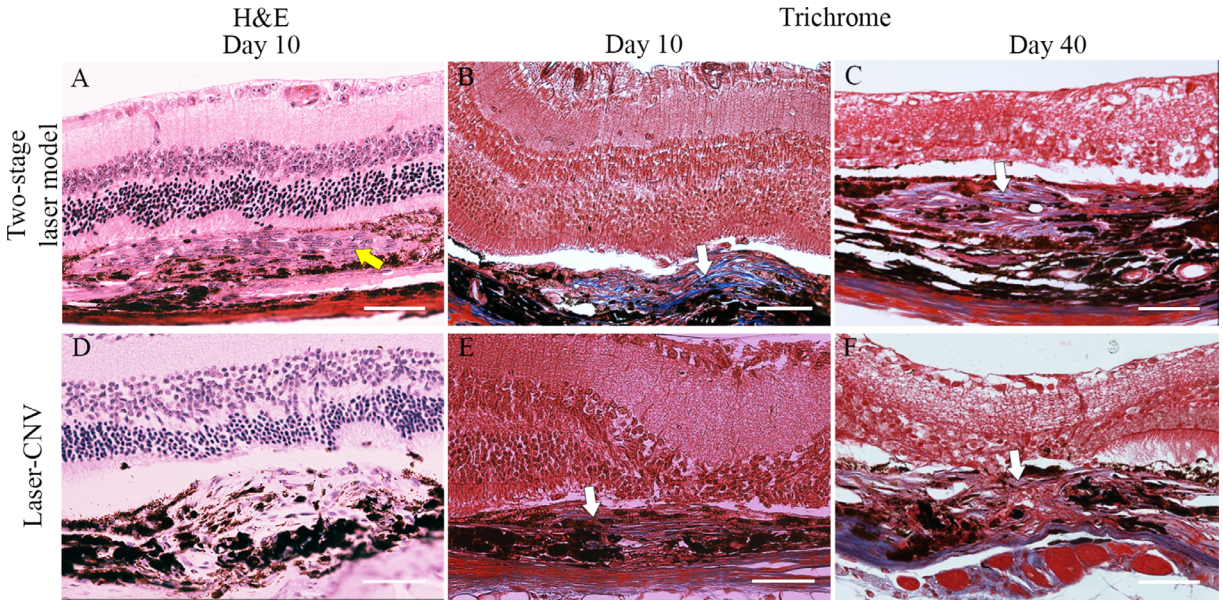

Figure 3. Histological observations of the subretinal lesion. Eyes were paraffin-embedded, sectioned, and stained with H&E or trichrome staining. (A) H&E staining showing subretinal lesion 10 days after the second laser treatment (A) and 10 days after traditional laser-CNV (D). Yellow arrow depicts cells within the sub-retinal lesion. Trichrome staining showing collagen deposition (blue) in subretinal lesion from the two-stage laser model at day 10 (B) or day 40 (C), and from the traditional laser-CNV model at day 10 (E) or day 40 (F). White arrows, collagen fibers. Scale bar = 100 µm.

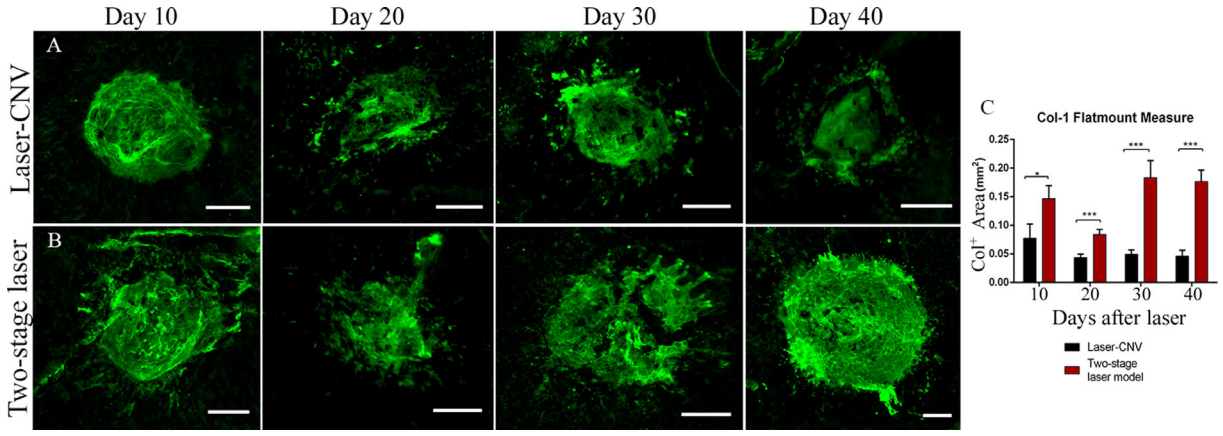

Figure 4. COL-1 deposition in subretinal lesions at different time points. RPE flatmounts from different days p.l-CNV or the second laser treatment were stained for COL-1. (A) Representative images of COL-1$^+$ lesions at 10, 20, 30, and 40 days after laser-CNV. (B) Representative images of COL-1$^+$ lesions at 10, 20, 30, and 40 days after two-stage laser model. (C) Comparison of COL-1$^+$ lesion area at different days between the traditional laser-CNV model and two-stage laser model. Mean ± SEM, N = 12–18 images (3–5 mice per group) *$P < 0.05$; ***$P < 0.001$, Student's *t*-test. Scale bar = 100 µm.

higher level of TGF-β expression was also observed in RPE/choroidal tissues from the two-stage laser model compared with that from controls (Fig. 7B).

The expression levels of fibrosis-related gene including COL-1, fibronectin, and α-SMA were significantly increased in the retinas from the two-stage laser mode compared with control (Fig. 7C). An increase was also observed in the traditional laser-induced CNV model for fibronectin and α-SMA genes (Fig. 7C). In the RPE/choroid (Fig. 7D), two-stage laser model had a significantly higher level of fibronectin expression compared with native controls. None of the other fibrotic genes were significantly upregulated in the RPE/choroid at this time point (25 days p.l) in the traditional one laser-induced model (Fig. 7D).

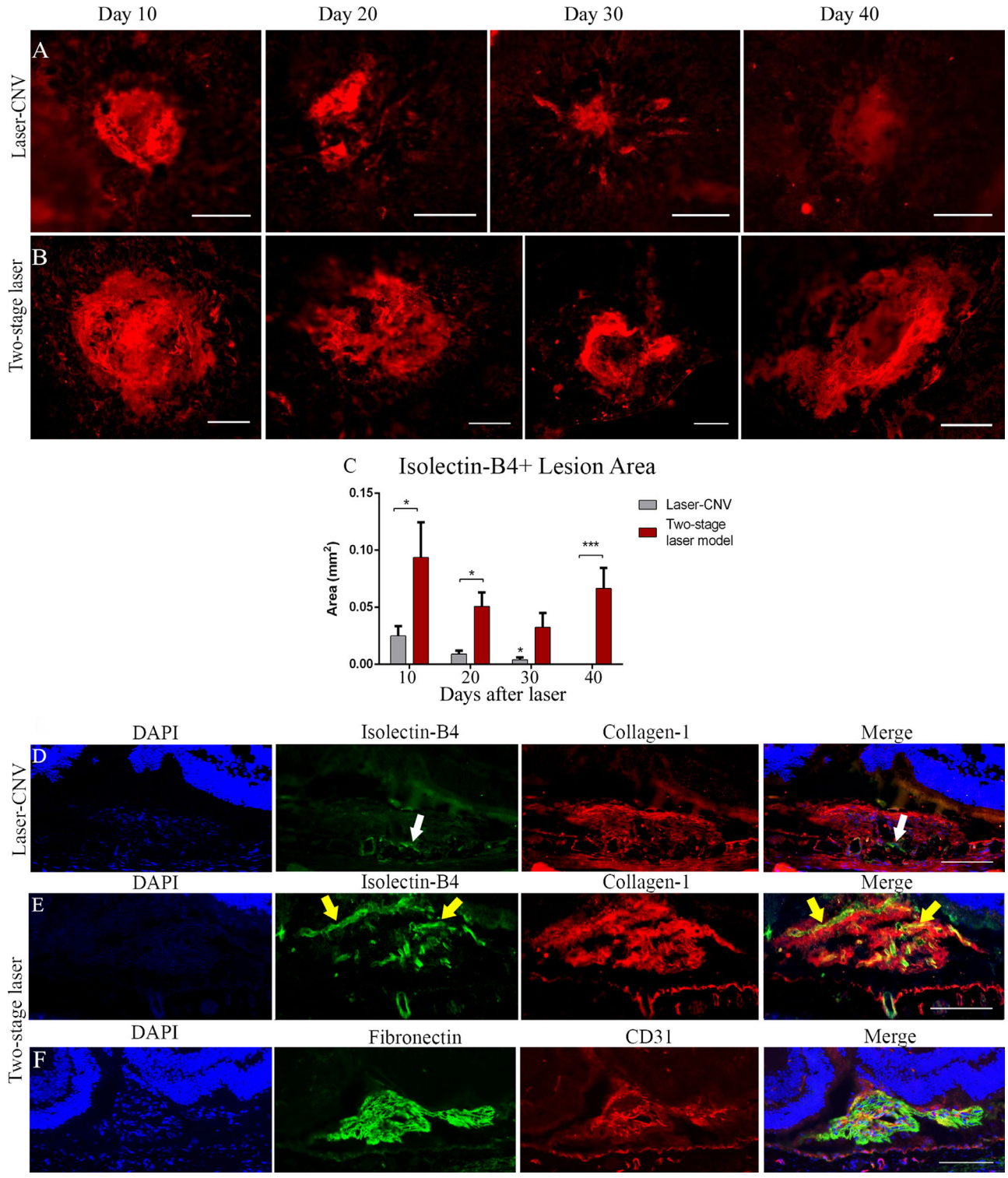

Figure 5. Vascular components of subretinal lesion in the two-stage laser-induced model. RPE flatmounts from different days p.l-CNV or the second laser treatment were stained for IB4. (A) IB4$^+$ lesions at different days after the traditional laser-CNV. (B) IB4$^+$ lesions at different days after two-stage laser model. (C) Comparison of IB4$^+$ area between laser-CNV model and two-stage laser model at different days. Mean $\pm$ SEM, N = 6–18 images (3–5 mice per group) *$P < 0.05$; ***$P < 0.001$, Student's *t*-test. Scale bar = 100 µm. (D, E) Cryosections of eyes from the traditional laser-CNV model (D) and two-stage laser model (E) 30 days p.l stained for COL-1 (red) and IB4 (green). White and yellow arrows indicate IB4$^+$ blood vessels. (F) Cryosections from two-stage laser model 30 days p.l stained for fibronectin (green) and CD31 (red). Scale bar = 100 µm.

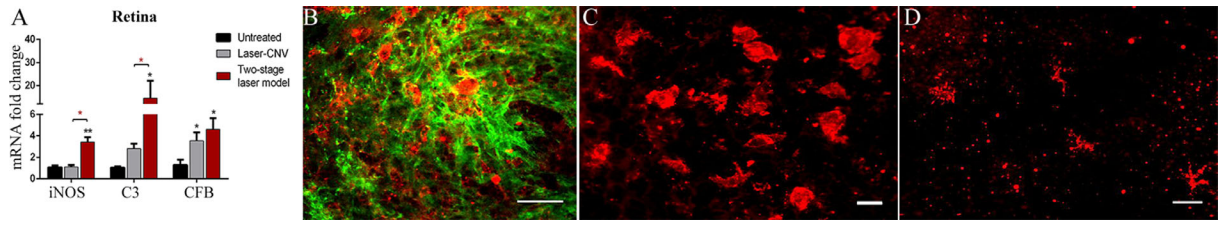

Figure 6. Inflammation in fibrovascular lesion. (A) RNA was extracted from retinal tissue 25 days p.l/post-second laser, and the expression of iNOS, C3, and CFB were investigated by real-time RT-PCR. Mean ± SEM, N = 6, Student's *t*-test, $*P < 0.05$; $**P < 0.01$. (B) Dual staining of F4/80$^+$ (red) and COL-1 (green) in RPE flatmount from day 30 p.l of the two-stage laser model showing F4/80$^+$ inside the fibrotic lesion. (C, D) Representative images showing F4-80$^+$ (red) cells in the RPE layer of two-stage laser model 30 days after the second laser burn (C) or 30 days after the traditional laser-CNV (D). Scale bar = 50 µm.

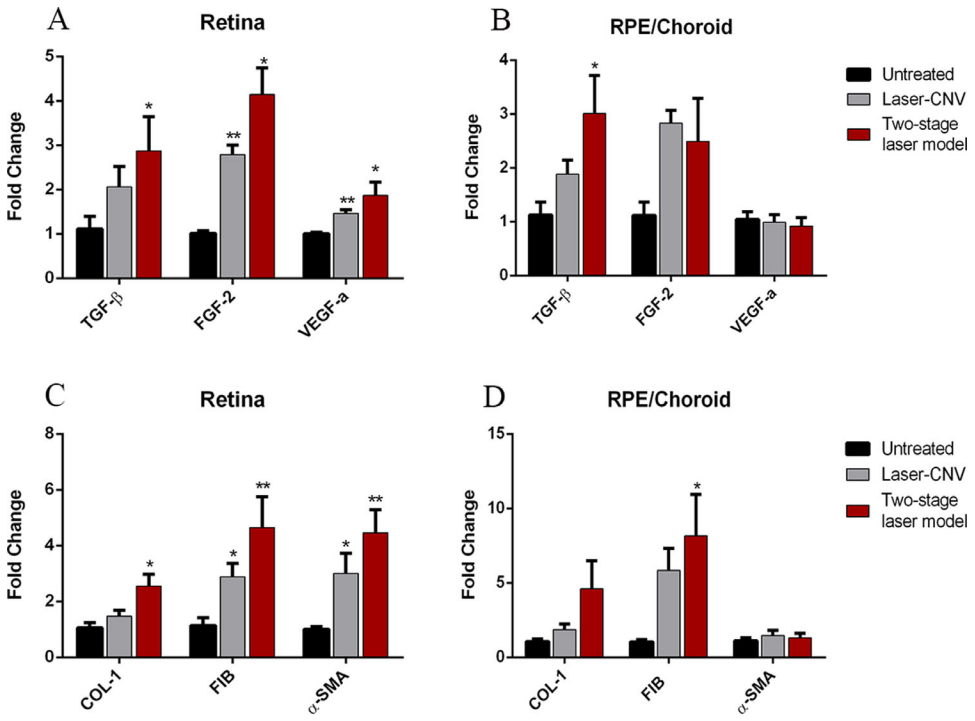

Figure 7. Two-stage laser model induces fibrotic gene expression. RNA was extracted from retina (A, C) and RPE/choroid (B, D) 25 days after laser/second laser and gene expression was examined by RT-PCR. (A, B) The expression of profibrotic growth factor genes (TGF-β, FGF2, and VEGF-a) in the retina and RPE/choroid. (C, D) The expression of fibrosis marker genes (COL-1, fibronectin, and α-smooth muscle actin). Mean ± SEM, N = 6, one-way ANOVA, Bonferroni corrected, $*P < 0.05$; $**P < 0.01$ compared with untreated control group.

Discussion

In this study, we described a two-stage laser-induced model of subretinal fibrosis that mirrors key aspects of macular fibrosis secondary to nAMD. First, the lesion arises from preexisting CNV. Second, the lesion does not regress (at least for 40 days) when remaining untreated. Most importantly, the lesion is highly vascularized and forms a fibrovascular membrane. Our model therefore is ideal for studying the pathogenesis of macular fibrosis and testing therapeutic compounds.

The late stage (e.g., 35 days) traditional laser-induced CNV has been used as a model to study the mechanisms of macular fibrosis and test therapeutic compounds.[9–12] We have found that the fibrotic component (COL-1) of the lesion reduces from day 10 to 20 p.l and remains unchanged afterward, whereas the vascular component (IB4$^+$ blood vessels) of the lesion progressively decreases and almost completely diminishes by day 40 p.l. Very few F4/80$^+$ macrophages were present around the lesion, and inflammatory genes (iNOS, C3, CFB; Fig. 6A) were mildly upregulated in the retina and RPE/choroid at day 25 p.l. Our results suggest that retinal lesion at the later stage of

this model is the result of wound-healing of the CNV. Because macular fibrosis in nAMD patients is highly vascularized[17] and contains various immune cells,[18] this traditional laser-induced CNV mediated subretinal fibrosis does not truthfully mirror the scenarios in nAMD patients.

The lesion in our two-stage laser-induced subretinal fibrosis remains vascularized evidenced by continued fluorescent leakage and the presence of $IB4^+$ (Fig. 5E) or $CD31^+$ (Fig. 5F) blood vessels. The lesion also has significant levels of inflammatory response evidenced by the huge number of immune cell infiltration and high levels of inflammatory genes expression. Our model therefore mirrors key features of macular fibrosis secondary to human nAMD and is suitable for mechanistic studies, as well as testing antifibrotic drugs.

In the two-stage laser model, the second laser was applied at day 7 when the CNV reaches to maximum size[7] and the laser burn was directed toward the CNV lesion. Approximately a third of lesions developed mild hemorrhage during the second laser treatment, although massive hemorrhage, which occurs occasionally in the traditional laser-induced CNV, was never observed. In theory, lesions with hemorrhage would have different inflammatory profiles from lesions without hemorrhage, hence different outcomes in retinal lesion. Interestingly, FFA and OCT examinations did not show any significant difference between lesions with and without hemorrhage (Figs. 1E, 2G, 2H). This may be explained by at least two reasons. First, the bleeding caused by the second laser is very mild (see Supplementary Fig. S1). Second, the second laser was applied to preexisting peak stage CNV that is already terribly inflamed, and an additional laser treatment would cause more severe inflammation regardless of a mild hemorrhage. Indeed, persistent inflammation was observed 20 to 30 days after the second laser treatment (Figs. 6, 7). Our results highlight the role of chronic inflammation in retinal fibrosis.

The dynamic changes in vascular component after the second laser treatment (decreased from day 10 to 30 and then increased on day 40) differ from that in fibrotic component (i.e., COL-1 deposition, decreased from day 10 to 20 and then increased afterword). This indicates that different cytokines and chemokines (proangiogenic vs. profibrotic) are involved in different types of retinal lesion in our model. Although the consistently present angiogenic component is a key feature of this model, VEGF expression was not increased in the two-stage laser model, compared with the traditional laser-induced CNV model (Fig. 7). It is possible that proangiogenic factors are upregulated at an earlier time point in the model, which we did not investigate. Alternatively, the angiogenic processes in this model may be propagated by other angiogenic factors independent of VEGF.

Immediately after the second laser treatment, the inflammatory response would further promote CNV. After the acute inflammatory response, the immune system and retinal tissue would try to control inflammation and promote tissue repair, which may result in reduced CNV (particularly blood vessels) and enhanced scar formation (collagen deposition). It appears that in our two-stage laser model, the levels of subretinal damage and its related inflammation exceed the repair capacity. As a result, subretinal inflammation persists and CNV turns into fibrovascular membrane.

Conclusions

The pathological events in our model mirror the clinical scenario whereby hemorrhage or sustained leakage occurs in nAMD patients. Macular hemorrhage[15] and refractory intraretinal cysts[14] are known risk factors of macular fibrosis in nAMD. Our model of subretinal fibrosis is a useful tool for dissecting the mechanisms contributing to subretinal fibrosis secondary to nAMD and testing antifibrotic drugs for nAMD patients.

Acknowledgments

This work is supported by Fight for Sight (5057/5058), the Department for the Economy (DfE) of Northern Ireland.

Disclosure: **K. Little,** None; **M. Llorian Salvador,** None; **M. Tang,** None; **X. Du,** None; **Ó. O'Shaughnessy,** None; **G. McIlwaine,** None; **M. Chen,** None; **H. Xu,** None

References

1. Wong WL, Su X, Li X, et al. Global prevalence of age-related macular degeneration and disease burden projection for 2020 and 2040: a systematic review and meta-analysis. *Lancet Glob Heal.* 2014;2:e106–e116.
2. Bloch SB, Lund-Andersen H, Sander B, Larsen M. Subfoveal fibrosis in eyes with neovascular age-related macular degeneration treated with intravitreal ranibizumab. *Am J Ophthalmol.* 2013;156:116–124.e1.

3. Miere A, Semoun O, Cohen SY, et al. Optical coherence tomography angiography features of subretinal fibrosis in age-related macular degeneration. *Retina*. 2015;35:2275–2284.
4. Little K, Ma JH, Yang N, Chen M, Xu H. Myofibroblasts in macular fibrosis secondary to neovascular age-related macular degeneration - the potential sources and molecular cues for their recruitment and activation. *EBioMedicine*. 2018;38:283–291.
5. Daniel E, Toth CA, Grunwald JE, et al. Risk of scar in the comparison of age-related macular degeneration treatments trials. *Ophthalmology*. 2014;121:656–666.
6. Tobe T, Ortega S, Luna JD, et al. Targeted disruption of the FGF2 gene does not prevent choroidal neovascularization in a murine model. *Am J Pathol*. 1998;153:1641–1646.
7. Lambert V, Lecomte J, Hansen S, et al. Laser-induced choroidal neovascularization model to study age-related macular degeneration in mice. *Nat Protoc*. 2013;8:2197–2211.
8. Ishikawa K, Kannan R, Hinton DR. Molecular mechanisms of subretinal fibrosis in age-related macular degeneration. *Exp Eye Res*. 2014;142:19–25.
9. Kwak N, Okamoto N, Wood JM, Campochiaro PA. VEGF is major stimulator in model of choroidal neovascularization. *Invest Ophthalmol Vis Sci*. 2000;41:3158–3164.
10. Bora PS, Sohn JH, Cruz JMC, et al. Role of complement and complement membrane attack complex in laser-induced choroidal neovascularization. *J Immunol*. 2005;174:491–497.
11. Nozaki M, Raisler BJ, Sakurai E, et al. Drusen complement components C3a and C5a promote choroidal neovascularization. *Proc Natl Acad Sci U S A*. 2006;103:2328–2333.
12. Zhang R, Liu Z, Zhang H, Zhang Y, Lin D. The COX-2-selective antagonist (NS-398) inhibits choroidal neovascularization and subretinal fibrosis. *PLoS One*. 2016;11:e0146808.
13. Jo YJ, Sonoda KH, Oshima Y, et al. Establishment of a new animal model of focal subretinal fibrosis that resembles disciform lesion in advanced age-related macular degeneration. *Investig Ophthalmol Vis Sci*. 2011;52:6089–6095.
14. Gianniou C, Dirani A, Jang L, Mantel I. Refractory intraretinal or subretinal fluid in neovascular age-related macular degeneration treated with intravitreal ranizubimab: functional and structural outcome. *Retina*. 2015;35:1195–1201.
15. Hwang JC, Del Priore L V, Freund KB, Chang S, Iranmanesh R. Development of subretinal fibrosis after anti-VEGF treatment in neovascular age-related macular degeneration. *Ophthalmic Surg Lasers Imaging*. 2011;42:6–11.
16. Chen M, Rajapakse D, Fraczek M, Luo C, Forrester JV, Xu H. Retinal pigment epithelial cell multinucleation in the aging eye–a mechanism to repair damage and maintain homoeostasis. *Aging Cell*. 2016;15:436–445.
17. Souied EH, Miere A, Cohen SY, Semoun O, Querques G. Optical coherence tomography angiography of fibrosis in age-related macular degeneration. *Dev Ophthalmol*. 2016;56:86–90.
18. Grossniklaus H. Histopathologic and ultrastructural findings of surgically excised choroidal neovascularization. Submacular Surgery Trials Research Group. *Arch Ophthalmol*. 1998;116:745–749.